RGMb protects against acute kidney injury by inhibiting tubular cell necroptosis via an MLKL-dependent mechanism

Wenjing Liu[a,b,1], Binbin Chen[a,1], Yang Wang[a], Chenling Meng[a], Huihui Huang[a], Xiao-Ru Huang[c], Jinzhong Qin[d], Shrikant R. Mulay[e], Hans-Joachim Anders[e], Andong Qiu[f], Baoxue Yang[g], Gordon J. Freeman[h], Hua Jenny Lu[i], Herbert Y. Lin[i], Zhi-Hua Zheng[j], Hui-Yao Lan[c], Yu Huang[a], and Yin Xia[a,k,2]

[a]School of Biomedical Sciences, Faculty of Medicine, The Chinese University of Hong Kong, Hong Kong, China; [b]School of Medicine, Yunnan University, Kunming, Yunnan 650091, China; [c]Department of Medicine and Therapeutics, Li Ka Shing Institute of Health Sciences, The Chinese University of Hong Kong, Hong Kong, China; [d]Ministry of Education Key Laboratory of Model Animal for Disease Study, Model Animal Research Center, Nanjing Biomedical Research Institute, Nanjing University, Nanjing 210014, China; [e]Medizinische Klinik und Poliklinik IV, Klinikum der Universität, München, Munich 80336, Germany; [f]School of Life Sciences and Technology, Tongji University, Shanghai 200092, China; [g]State Key Laboratory of Natural and Biomimetic Drugs, Department of Pharmacology, School of Basic Medical Sciences, Peking University, Beijing 100191, China; [h]Department of Medical Oncology, Dana–Farber Cancer Institute, Harvard Medical School, Boston, MA 02215; [i]Division of Nephrology, Program in Membrane Biology, Center for Systems Biology, Department of Medicine, Massachusetts General Hospital, Harvard Medical School, Boston, MA 02114; [j]Department of Nephrology, The Seventh Affiliated Hospital, Sun Yat-sen University, Shenzhen 518107, China; and [k]Key Laboratory for Regenerative Medicine, Ministry of Education, School of Biomedical Sciences, Faculty of Medicine, The Chinese University of Hong Kong, Hong Kong, China

Edited by Xiaodong Wang, National Institute of Biological Sciences, Beijing, China, and approved January 5, 2018 (received for review September 29, 2017)

Tubular cell necrosis is a key histological feature of acute kidney injury (AKI). Necroptosis is a type of programed necrosis, which is executed by mixed lineage kinase domain-like protein (MLKL) upon its binding to the plasma membrane. Emerging evidence indicates that necroptosis plays a critical role in the development of AKI. However, it is unclear whether renal tubular cells undergo necroptosis in vivo and how the necroptotic pathway is regulated during AKI. Repulsive guidance molecule (RGM)-b is a member of the RGM family. Our previous study demonstrated that RGMb is highly expressed in kidney tubular epithelial cells, but its biological role in the kidney has not been well characterized. In the present study, we found that RGMb reduced membrane-associated MLKL levels and inhibited necroptosis in cultured cells. During ischemia/reperfusion injury (IRI) or oxalate nephropathy, MLKL was induced to express on the apical membrane of proximal tubular (PT) cells. Specific knockout of Rgmb in tubular cells (Rgmb cKO) increased MLKL expression at the apical membrane of PT cells and induced more tubular cell death and more severe renal dysfunction compared with wild-type mice. Treatment with the necroptosis inhibitor Necrostatin-1 or GSK′963 reduced MLKL expression on the apical membrane of PT cells and ameliorated renal function impairment after IRI in both wild-type and Rgmb cKO mice. Taken together, our results suggest that proximal tubular cell necroptosis plays an important role in AKI, and that RGMb protects against AKI by inhibiting MLKL membrane association and necroptosis in proximal tubular cells.

acute kidney injury | necroptosis | RGMb | proximal tubular cells | MLKL

Acute kidney injury (AKI) is characterized by rapid declines in kidney functions within 1 wk. AKI affects millions of patients worldwide with high mortality, morbidity, and cost. Unfortunately, no effective treatment strategies for AKI are available due to insufficient understanding of the underlying mechanisms (1).

Acute tubular necrosis is a key histological feature of AKI. However, previous studies were directed toward apoptosis because apoptosis was considered to be the only genetically programmed and therapeutically alterable form of cell death in AKI, while necrosis was thought to be a nonregulated response to overwhelming stress (2). Apoptosis following renal ischemia/reperfusion injury (IRI) was first described in 1992 (3), and subsequently it was shown that blockade of apoptosis with IGF1 or the pan caspase inhibitor Z-VAD-FMK (zVAD)-fmk prevented renal function impairment after ischemia (4). The importance of apoptosis in the development of AKI, however, was challenged by recent studies showing that cleaved caspase-3 was not detectable in injured kidneys and that administration of zVAD-fmk had no effects on renal injury after IR or folic acid overdose (5–7).

Studies in the past decade or so have found that necrosis can be a regulated or programmed process in various pathological and physiological conditions (8–12). Receptor-interacting protein kinase (RIP) 1 and RIP3-mediated necroptosis (8, 11, 13) is the best-studied regulated necrosis pathway. Unlike apoptosis, necroptosis is caspase-independent programmed cell death. Many extrinsic signals such as TNF-α, FAS ligand, interferons, Toll-like receptor (TLR) ligands, and various pathogen components can trigger necroptosis upon perturbation of caspase-8–mediated apoptosis. Necroptosis involves the formation of the necroptosome, a necroptosis-inducing complex containing RIP1, RIP3, and mixed lineage kinase domain-like protein (MLKL). Within this complex, RIP1 phosphorylates RIP3, and RIP3 then recruits and phosphorylates its substrate MLKL. Phosphorylation of MLKL triggers its oligomerization and membrane translocation, which are necessary and sufficient for the induction of necrosis (14–23).

MLKL consists of an N-terminal four-helical bundle domain (4HBD) fused by a brace region to a C-terminal pseudokinase domain. The 4HBD of MLKL is structurally similar to α-pore–forming

Significance

Necroptosis is critically involved in the development of acute kidney injury (AKI), but it has not been well demonstrated that necroptosis occurs in renal tubular epithelial cells in vivo during AKI. Now, we provide evidence that renal proximal tubular cells undergo necroptosis during ischemia/reperfusion injury or oxalate nephropathy. Repulsive guidance molecule-b protects against AKI by inhibiting mixed lineage kinase domain-like membrane association and necroptosis in proximal tubular cells.

Author contributions: W.L., B.C., C.M., H.H., J.Q., A.Q., B.Y., H.J.L., Z.-H.Z., H.-Y.L., Y.H., and Y.X. designed research; W.L., B.C., Y.W., C.M., H.H., and Y.X. performed research; X.-R.H., S.R.M., H.-J.A., A.Q., B.Y., G.J.F., H.J.L., H.Y.L., Z.-H.Z., H.-Y.L., and Y.H. contributed new reagents/analytic tools; W.L., B.C., Y.W., C.M., H.H., J.Q., Z.-H.Z., and Y.X. analyzed data; and W.L., B.C., X.-R.H., J.Q., B.Y., G.J.F., H.J.L., H.Y.L., Z.-H.Z., H.-Y.L., Y.H., and Y.X. wrote the paper.

The authors declare no conflict of interest.

This article is a PNAS Direct Submission.

Published under the PNAS license.

[1]W.L. and B.C. contributed equally to this work.

[2]To whom correspondence should be addressed. Email: xia.yin@cuhk.edu.hk.

This article contains supporting information online at www.pnas.org/lookup/suppl/doi:10.1073/pnas.1716959115/-/DCSupplemental.

toxins, and is sufficient to oligomerize, bind to phosphatidylinositol lipids through a patch of positively charged amino acids, permeabilize the plasma membrane, and trigger cell death (20, 21, 23–25). However, the activation of the full-length MLKL requires phosphorylation of Thr357 and Ser358 in human MLKL (17, 23), or Ser345 and Ser347 in mouse MLKL (26, 27), to unleash the 4HBD for oligomerization and membrane recruitment of MLKL and subsequent membrane rupture (24).

Physiologically relevant necroptosis has been found in T lymphocytes (28), photoreceptors (29), microglia (30), and enterocytes (31). Necroptosis has also been shown to contribute to the pathogenesis of ischemic injury in the brain, heart, and kidney (5, 6, 8, 32, 33), atherosclerosis (34), pancreatitis (14), inflammatory bowel diseases (35), and viral infection (36). In renal IRI, necroptosis appears to be predominant over apoptosis, and necroptosis contributes to IRI as genetic deletion of Rip3 or inhibition of RIP1 kinase by necrostatin-1 (Nec-1) each prevented renal injury (5, 6). In addition, a recent study demonstrated that acute crystal nephropathy involves RIP3-MLKL–mediated necroptosis (37). It has been well documented that tubular cells undergo necroptosis in vitro (5, 6, 37, 38). However, since the previous studies used Nec-1 administration, or global Rip3 or Mlkl knockout mouse models, it is unclear whether necroptosis occurs in renal tubular cells in vivo during AKI (6, 37, 38).

Repulsive guidance molecules b (RGMb) is a member of the RGM family, which consists of RGMa, RGMb, and RGMc (hemojuvelin). The RGM proteins associate with cell membrane through a glycophosphatidylinositol (GPI) anchor, and have been shown to be coreceptors for BMP signaling as well as ligands for the neogenin receptor (39). RGMb, also known as Dragon, was originally identified through a genomic screen for genes regulated by the transcription factor DRG11 in embryonic dorsal root ganglion (40). The biological functions of RGMb are only beginning to emerge. Our previous study demonstrated that homozygous RGMb-deficient mice die at early postnatal ages and that RGMb inhibits IL-6 expression in macrophages through the BMP pathway (41). RGMb also promotes neurite outgrowth and peripheral nerve regeneration by modulating BMP signaling (42). In addition, RGMb binds to PD-L2, and this interaction promotes respiratory tolerance (43).

We previously showed that RGMb is highly expressed in the tubular epithelial cells of the kidney (44). Using heterozygous global Rgmb knockout mice, we were able to demonstrate that RGMb induces apoptosis in the tubular cells of kidneys subjected to unilateral ureteric obstruction (UUO) (45), but this regulation was not observed in renal IRI. To further identify the specific role of RGMb in renal tubular cells during AKI, we generated renal tubular cell-specific Rgmb knockout mice. We found that RGMb protects kidneys from IRI and oxalate nephropathy by inhibiting necroptosis in proximal tubular cells.

Results

Tubule-Specific Ablation of Rgmb Aggravates AKI Induced by IR. Our previous study demonstrated that RGMb is highly expressed in renal tubular cells including proximal tubular cells (44). To examine the specific role of RGMb in renal tubules, we generated renal tubule-specific Rgmb knockout mice by interbreeding floxed Rgmb mice (46) with Ksp-Cre mice (*SI Appendix*, Fig. S1). Ksp-Cre has been shown to efficiently ablate floxed Smad2, β-catenin, and Dicer in renal tubules including proximal tubules (47–49), although Cre recombinase is expressed at lower levels in proximal tubules compared with collecting ducts and thick ascending limbs (50).

Rgmb mRNA was reduced by 65% in Rgmb cKO kidneys compared with wild-type (WT) kidneys (*SI Appendix*, Fig. S2*A*), while RGMb protein, the specificity of which was determined by the kidney sample from a global Rgmb KO (gKO) mouse, was reduced by 67% (*SI Appendix*, Fig. S2*B*). As previously demonstrated by us (44), RGMb was highly expressed in various renal tubules including proximal tubules (marked by megalin), and this expression was markedly reduced in Rgmb cKO kidneys (*SI Appendix*, Fig. S2 *C* and *D*).

Rgmb cKO mice appeared to be grossly normal. Rgmb cKO mice showed normal kidney sizes and structures, and normal serum creatinine levels. Therefore, RGMb is not critical for normal kidney function.

We next examined the effects of Rgmb ablation on acute tubular injury after IR. Compared with WT mice, Rgmb cKO mice exhibited more severe tubular injury, characterized by loss of brush border, tubular dilation, tubular cell depletion, and cast formation in the lumen of tubules, 24 h after IR (Fig. 1*A*). Overall tubular injury scores were higher in Rgmb cKO than in WT mice (Fig. 1*B*). Ngal, a marker for kidney injury (51), in the kidney and urine, was increased in Rgmb cKO mice compared with WT mice (Fig. 1 *C* and *D*). Urinary chromatin protein high mobility group B1 (HMGB1), a marker of necrosis (52), was also increased in Rgmb cKO after IR (Fig. 1*D*). More TUNEL-positive cells were observed in Rgmb cKO than in WT kidneys (Fig. 1*E*). The inflammatory factors Il-6, Cxcl-1, Cxcl-2, and TNF-α was up-regulated by IR. Deletion of Rgmb further increased the expression of Il-6, Cxcl-1, and Cxcl-2, but not TNF-α (Fig. 1 *F*–*I*). Serum creatinine and blood urea nitrogen (BUN) levels were significantly higher in Rgmb cKO mice than in WT mice (Fig. 1 *J* and *K*). Taken together, it is clear that the loss of Rgmb in tubular cells aggravates IRI.

RIP3 and MLKL Expression in the Kidney Are Induced by IRI. To investigate the types of cell death regulated by RGMb, we examined the expression levels of the key regulators in cell death. Cleaved caspase-3 and cleaved PARP were not altered in kidneys collected 12 and 24 h after ischemia in both WT and Rgmb cKO mice compared with the sham control. As positive control, cleaved caspase-3 and cleaved PARP were increased by UUO (*SI Appendix*, Fig. S3 *A* and *B*). These results suggest that the increased cell death in Rgmb cKO kidneys during IRI may not be apoptosis. Conversion of LC3-I into LC3-II did not significantly change following IRI. P62 appeared to be slightly increased upon ischemia, but there were no differences between WT and Rgmb cKO mice (*SI Appendix*, Fig. S4). Therefore, autophagy is not a mechanism underlying RGMb's protective role.

Ferroptosis is an iron-dependent form of necrosis that occurs due to lipid peroxidation. System x^-_c and GPX4 are the two known key regulators of ferroptosis, and inhibition of either Slc7a11, a subunit of the system x^-_c, or GPX4 induces ferroptosis (53, 54). Interestingly, Slc7a11 and Gpx4 expression was markedly increased by IR and there was no significant difference in the expression of the two genes between WT and Rgmb cKO mice (*SI Appendix*, Fig. S5), indicating that ferroptosis may not be a mechanism of RGMb action.

Critical for the formation of the necroposome is a comprised caspase-8 activity (55, 56). Interestingly, cleaved caspase-8 was reduced 12 and 24 h after ischemia (Fig. 2 *A* and *B*). Rip1 mRNA in the kidney was slightly up-regulated 12 h after ischemia, and was slightly down-regulated 24 h after ischemia (Fig. 2*C*) in both WT and Rgmb cKO mice, with no difference between the two genotypes. Rip3 and Mlkl mRNA levels increased 12 and 24 h after ischemia (Fig. 2 *D* and *E*). RIP3 protein was barely detectable in sham-operated kidneys, but markedly increased 12 and 24 h (Fig. 2*F*) after ischemia. MLKL protein did not change 12 h after ischemia, but increased 24 h after ischemia (Fig. 2*G*). Both MLKL mRNA and protein levels were similar between WT and cKO kidneys 24 h after ischemia (Fig. 2 *E* and *G*). These results suggest that the necroptotic pathway may be activated by IR.

IR and Deletion of Rgmb Promote Expression of MLKL in the Apical Membrane of Proximal Tubular Cells. To determine the cell types that may undergo necroptosis during IRI, we examined cellular localization of RIP3 and MLKL by immunofluorescence. RIP3 was not detectable in sham-operated kidneys, but was readily detected in proximal tubules in cortex and outer medulla 12 and 24 h after ischemia. No RIP3 expression was found in other tubules

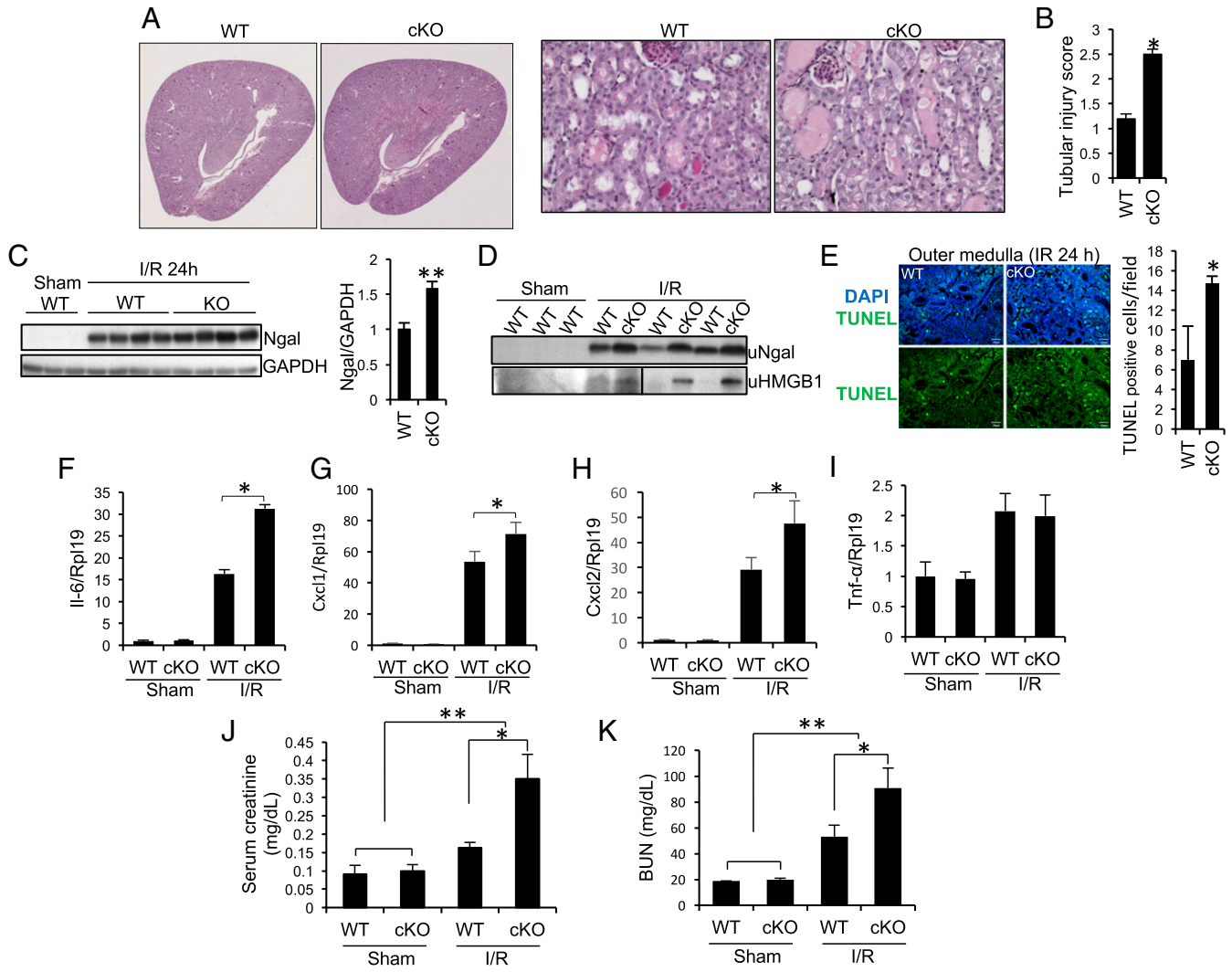

Fig. 1. Tubule-specific ablation of Rgmb aggravates IRI. Male WT and Rgmb cKO mice at 2 mo of age underwent 40 min of bilateral renal pedicle clipping. Mice were killed 24 h after reperfusion. (*A*) Periodic acid-Schiff (PAS) staining of kidney sections from WT and Rgmb cKO mice after IR. Representative photographs at different magnifications show more brush border loss, tubular dilation, tubular cell depletion, and cast formation in Rgmb cKO mice than in WT mice. (*B*) Quantitative assessment of tubular injury is presented. (*C*) Expression of Ngal in the kidneys of WT and Rgmb cKO after IR. Kidney lysates from sham-operated kidneys and injured kidneys were subjected to Western blotting for Ngal (*Left*), and quantified by densitometry (*Right*). (*D*) Excreted Ngal and HMGB1 in urine (uNgal and uHMGB1). Spot urinary samples were collected from sham-operated mice and mice with IR when they were killed. The same volume of samples was used for Western blotting. (*E*) TUNEL-positive tubular cells in outer medulla. Paraffin kidney sections from WT and Rgmb cKO mice were used for TUNEL staining (*Left*). Nuclear localization of TUNEL signal was demonstrated by cyan-colored nuclei after merging with DAPI. Positive tubular epithelial cells in each field were counted (*Right*). (*F–I*) Expression of inflammatory factors in the kidney. Kidney lysates from sham-operated kidneys and injured kidneys were used for real-time PCR analysis for Il-6, Cxcl1, Cxcl2, and Tnf-α. (*J* and *K*) Serum creatinine and BUN levels in sham-operated mice and in mice with IR. Rpl19 was used as the internal control for real-time PCR. GAPDH was used as the loading control for Western blotting. $n = 6–8$ for *B* and *F–K*; $n = 3$ for *E*. $^*P < 0.05$; $^{**}P < 0.01$.

(*SI Appendix*, Figs. S6 and S7). Similar staining pattern was obtained when a different RIP3 antibody was used (*SI Appendix*, Fig. S8). There was no appreciable difference in RIP3 signal between WT and Rgmb cKO mice (*SI Appendix*, Figs. S6 and S7).

We then examined the so-far most-terminal known end-stage effector of the necroptosis pathway MLKL. MLKL was detected only in collecting ducts (positive for AQP2) in a diffused manner in sham-operated kidneys and in injured kidneys collected 12 h after ischemia in WT and Rgmb cKO mice (*SI Appendix*, Fig. S9). Twenty-four hours after IR, in addition to the expression in collecting duct (*SI Appendix*, Fig. S10), MLKL was also found to be expressed in the apical membrane of proximal tubules in inner cortex and outer medulla 24 h after ischemia (Fig. 3*A*). Strikingly, MLKL apical staining in proximal tubules was much increased in Rgmb cKO kidneys compared with WT kidneys (Fig. 3*A*). No apparent MLKL signal was found in the proximal tubules in the outer cortex (*SI Appendix*, Fig. S10).

We also extracted membrane proteins from the cortex and outer medulla of injured kidneys of WT and Rgmb cKO mice (Fig. 3*B*). Membrane-associated MLKL levels were increased in Rgmb cKO compared with WT kidneys, whereas cytosolic MLKL was similar between the two genotypes (Fig. 3*B*). Since translocation of MLKL to the plasma membrane is an indicator of MLKL activation and necroptosis. Our results suggest that necroptosis is induced in proximal tubules by IR, and deletion of RGMb promotes IRI-induced necroptosis.

Ablation of Rgmb Increases Apical MLKL Expression in Proximal Tubules and Aggravates AKI Induced by Oxalate Crystals. Crystal nephropathy also involves RIP3-MLKL–mediated necroptosis (37). To confirm

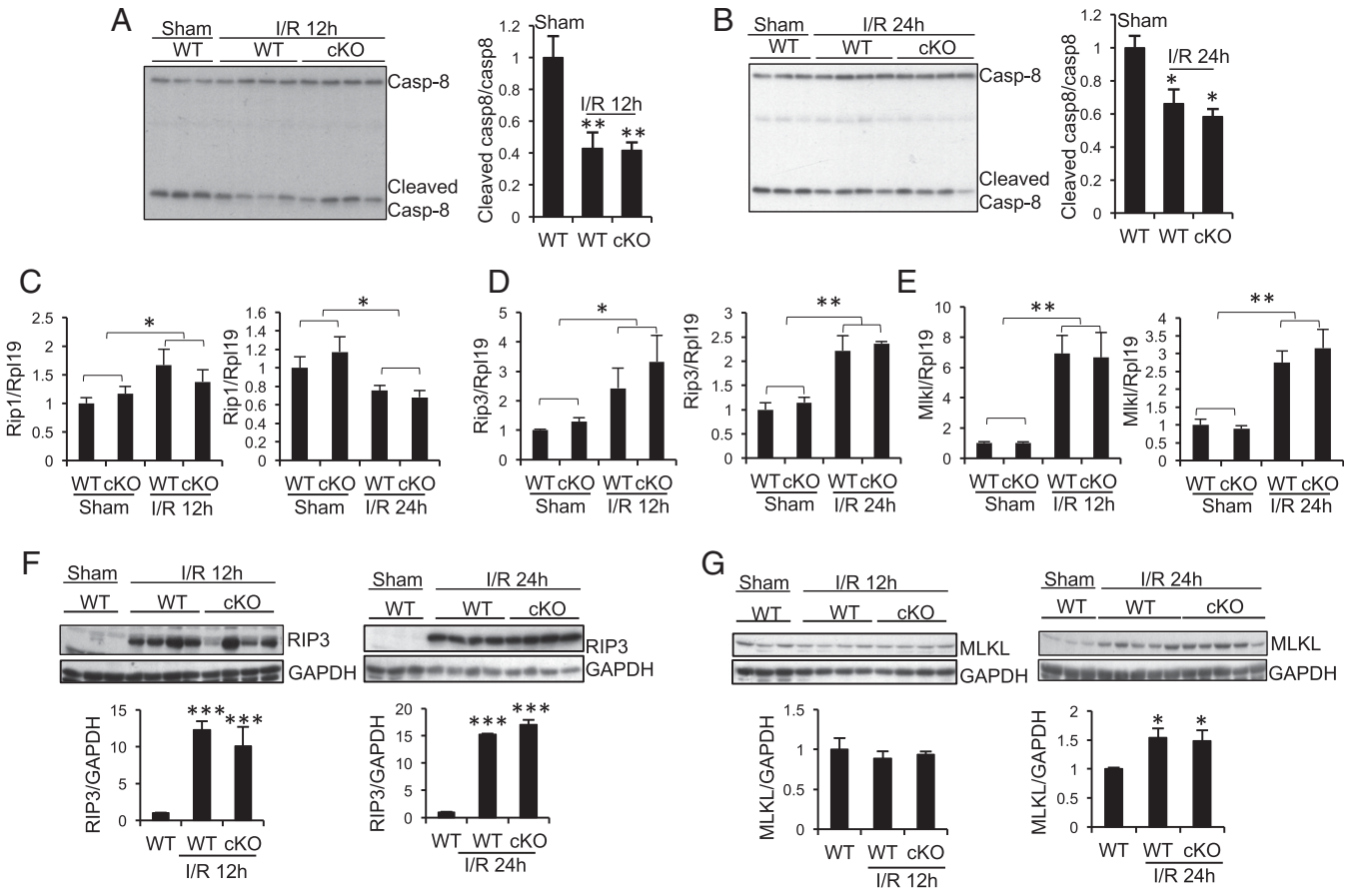

Fig. 2. Changes in expression of cleaved caspase-8, RIP1, RIP3, and MLKL in the kidneys of WT and Rgmb cKO mice after IRI. Male WT and Rgmb cKO mice at 2 mo of age underwent 40 min of bilateral renal pedicle clipping. Mice were killed after 12 and 24 h. (*A* and *B*) Cleaved caspase-8 levels in kidneys 12 and 24 h after IR. Kidney lysates 12 (*A*) and 24 h (*B*) after reperfusion were subjected to Western blotting using an antibody that recognizes both full-length and cleaved caspase-8 (Casp-8). Cleaved caspase-8 levels relative to full-length caspase-8 levels were quantified by densitometry. (*C*–*E*) mRNA levels of Rip1, Rip3, and Mlkl in kidneys 12 and 24 h after IR. Kidneys collected from WT and cKO mice subjected to sham operation or IR were analyzed for mRNA levels of Rip1 (*C*), Rip3 (*D*), and Mlkl (*E*) by real-time PCR. (*F* and *G*) Protein levels of RIP3 and MLKL in kidneys 12 and 24 h after IR. Kidneys collected from WT and cKO mice subjected to sham operation and IR were analyzed for protein levels of RIP3 (*F*) and MLKL (*G*) by Western blotting. RIP3 and MLKL levels relative to GAPDH levels were quantified by densitometry. Rpl19 was used as the internal control for real-time PCR. GAPDH was used as the loading control for Western blotting. $n = 5$–6 for *C*–*E*. $^{*}P < 0.05$; $^{**}P < 0.01$; $^{***}P < 0.001$.

RGMb's role in tubular cell necroptosis during AKI, we induced crystal nephropathy by a single injection of NaOx. Intrarenal calcium oxalate (CaOx) crystal deposition was similar between WT and Rgmb cKO mice 24 h after NaOx injection (*SI Appendix*, Fig. S11). Serum creatinine and BUN levels were higher in Rgmb cKO than in WT mice (Fig. 4*A*). Histologically, more tubular damage and higher kidney injury scores were found in Rgmb cKO than in WT mice (Fig. 4*B*). Urinary Ngal levels were also increased in Rgmb cKO mice compared with WT mice (Fig. 4*C*).

Cleaved caspase-8 was reduced in kidneys after NaOx treatment in both WT and Rgmb cKO mice (Fig. 4*D*). RIP3 and MLKL in the whole kidney were induced by NaOx treatment (Fig. 4*E*). Weak RIP3 staining was found in proximal tubular cells in both WT and Rgmb cKO kidneys injected with NaOx, with no apparent difference between the two genotypes (*SI Appendix*, Fig. S12). MLKL was localized to the apical membrane of proximal tubular cells in the cortex and outer medulla of injured kidneys of WT mice, and this expression was increased in Rgmb cKO mice (Fig. 4*F*). MLKL levels in membrane fractions were increased by NaOx treatment and further increased by Rgmb deletion (*SI Appendix*, Fig. S13). These results suggest that, as in the IRI model, loss of RGMb induced more MLKL membrane expression in proximal tubules and exacerbated tubular injury and renal dysfunction in the oxalate nephropathy.

Inhibition of Necroptosis Reduces MLKL Apical Expression in Proximal Tubules and Ameliorates Tubular Injury and Renal Function Impairment After IR. To determine the contributions of proximal tubular cell necroptosis and its regulation by RGMb to IRI, we treated WT and Rgmb cKO mice with the necroptosis inhibitor Nec-1 30 min before IR. In mice injected with the vehicle (DMSO), deletion of Rgmb increased serum creatinine levels 24 after IR (Fig. 5*A*, compare bars 4 and 3). Treatment with Nec-1 reduced serum creatinine levels in both WT and Rgmb cKO mice, which were no longer different between the two genotypes (Fig. 5*A*, bars 5 and 6). Nec-1 also improved the tubular injury in both WT and Rgmb cKO kidneys after IR (Fig. 5*B*). These results confirm the previous finding that necroptosis contributes to IRI (5, 6), and also suggest that RGMb inhibits necroptosis during IRI.

Nec-1 did not significantly alter MLKL expression in the kidney (Fig. 5*C*). Intriguingly, Nec-1 blocked the translocation of MLKL to the apical membrane in proximal tubules in both WT and Rgmb cKO kidneys (Fig. 5*D*). Consistently, MLKL levels in membrane fractions induced by IR were reduced by Nec-1 treatment (Fig. 5*E*).

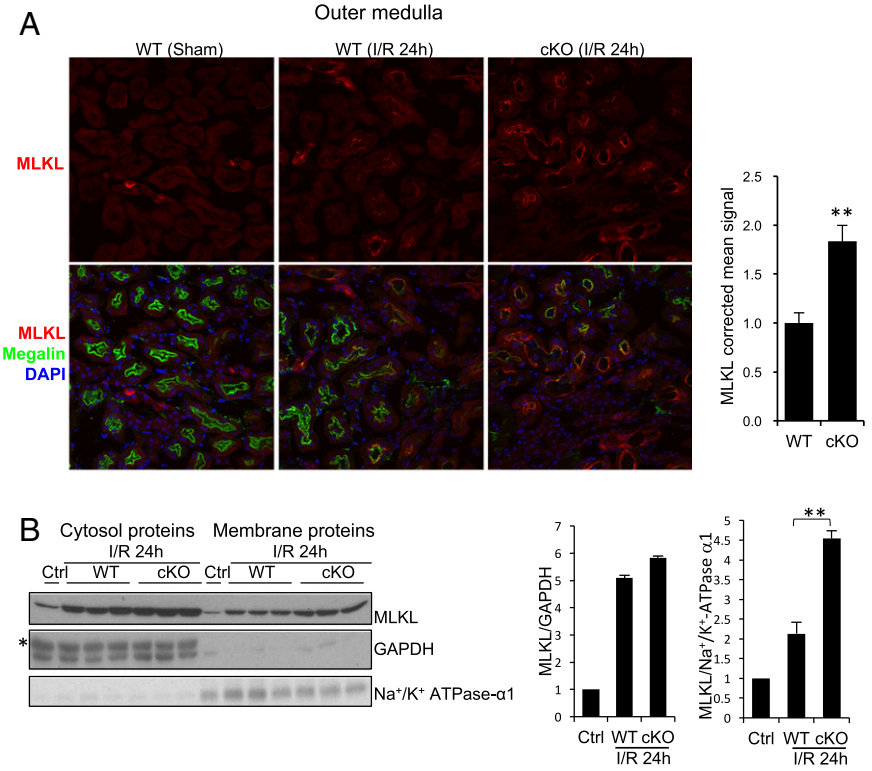

Fig. 3. Cellular localization of MLKL in WT and Rgmb cKO kidneys after IRI. (*A*) MLKL localization in the outer medulla. Immunofluorescence was performed on sections from sham-operated kidneys and kidneys of WT and Rgmb cKO mice 24 h after ischemia (40 min) and reperfusion for MLKL. Costaining with megalin was included to identify proximal tubules. Outer medulla is presented. MLKL apical signal was quantified by ImageJ. Five mice were used for each group for MLKL quantification. (*B*) MLKL levels in cytosolic and membrane fractions of kidneys. Membrane proteins and cytosolic proteins were isolated from the cortex and outer medulla of control kidneys or kidneys of WT and Rgmb cKO mice with IRI, and subjected to Western blotting for MLKL (*Left*). MLKL relative to GAPDH in cytosolic fractions and MLKL relative to α1-subunit of Na^+/K^+ ATPase in membrane fractions were quantified by densitometry (*Right*). GAPDH was used as the loading control for cytosolic samples, and α1-subunit of Na^+/K^+ ATPase was used as the control for membrane proteins. $^{**}P < 0.01$.

GSK′963, another necroptosis inhibitor structurally distinct from Nec-1 (57), also reduced the serum creatinine levels and apical MLKL signal in proximal tubules in WT and Rgmb cKO mice (*SI Appendix*, Fig. S14). These results further support that MLKL-mediated and RGMb-regulated necroptosis occurs in proximal tubules during IRI.

RGMb Inhibits Necroptosis in TKPTS, HT-29, and HK-2 Cells. To directly examine whether RGMb regulates necroptosis, we used TKPTS mouse proximal tubular cells, which have been reported to be sensitive to TNF-α/cycloheximide (CHX)/zVAD-fmk–induced cell death, a classical assay for necroptosis (5). Consistent with this previous observation, a combination of TNF-α, CHX, and zVAD-fmk (TCZ) induced more cell death than TNF-α plus CHX (TC) as determined by ATP levels (Fig. 6*A*). Cotreatment with Nec-1 decreased cell death induced by TCZ, thus defining the cell death induced by TCZ as RIP1-dependent necroptosis (Fig. 6*A*). We then transfected TKPTS cells with increasing amounts of RGMb cDNA. RGMb did not have any effects on TC-induced cell death (apoptosis), but dose-dependently inhibited TCZ-induced necroptosis (Fig. 6*B*). RGMb also reduced TCZ-induced release of HMGB1 into the cell culture media (Fig. 6*C*), while it did not affect HMGB1 mRNA expression (*SI Appendix*, Fig. S15*B*). RGMb did not alter Rip1, Rip3, and Mlkl expression after TCZ treatment (*SI Appendix*, Fig. S15 *C–E*). These results suggest that RGMb inhibits necroptosis in TKPTS cells.

We also used HT-29 colonic epithelial cells, a widely used necroptosis-sensitive cell line, to further examine RGMb's role in necroptosis. As shown in Fig. 6*D*, HT-29 underwent drastic necroptosis in the presence of TNF-α, the Smac mimetic Birinapant and zVAD-fmk (TSZ). RGMb markedly inhibited TSZ-induced necroptosis while it did not affect TS-induced apoptosis (Fig. 6 *E* and *F*). Inhibition of RGMb expression by two shRNA sequences increased TSZ-induced necroptosis, and these increases were abolished by cotransfection with Rgmb cDNA (*SI Appendix*, Fig. S16). These results further indicate that RGMb inhibits necroptosis in HT-29 cells.

A recent study found that crystals induce necroptosis in renal tubular cells (37). Consistent with this study, CaOx crystals induced cell death in HK-2 human proximal tubular cells, and this effect was blocked by Nec-1 (Fig. 6*G*). RGMb overexpression dose-dependently inhibited CaOx-induced cell death (Fig. 6*H*), suggesting a role of RGMb in inhibiting CaOx-induced necroptosis.

To determine whether the GPI anchor is necessary for RGMb activity, we generated chimeric Rgmb-TM, in which the GPI anchor is replaced with the transmembrane (TM) domain from platelet-derived growth factor receptor, thus RGMb is anchored to the membrane via the TM domain. The proteins of Rgmb-TM expressed at the expected molecular weights and was able to stimulate BMP signaling as WT Rgmb did (*SI Appendix*, Fig. S17). Interestingly, RGMb-TM also dose-dependently inhibited TSZ-induced necroptosis in HT-29 cells (Fig. 6*I*). These results suggest that Rgmb activity is not dependent on the presence of GPI anchor, but rather on the localization on the plasma membrane.

RGMb Reduces Plasma Membrane-Associated MLKL. MLKL phosphorylation, oligomerization, and plasma membrane translocation are the key steps for MLKL to execute necroptosis. We therefore examined whether RGMb regulates these modifications on MLKL. HT-29 cells transfected with Rgmb were treated with TSZ for 3 or 6 h. TSZ induced MLKL phosphorylation (Thr357) 3 h or 6 h after TSZ treatment (Fig. 7 *A* and *B*). MLKL oligomerization was detected at 6 h (Fig. 7*B*) but not at 3 h (data not shown) after TSZ treatment. Both MLKL phosphorylation and oligomerization were inhibited by Nec-1 (Fig. 7 *A* and *B*). RGMb overexpression did not alter MLKL phosphorylation and oligomerization (Fig. 7 *A* and *B*).

Once oligomerized, MLKL translocates to the plasma membrane to induce cell membrane rupture and cell death. TSZ increased membrane-associated MLKL as determined by either total MLKL or phosphorylated MLKL (Fig. 7*C*). Membrane-associated MLKL was significantly reduced in the presence of RGMb (Fig. 7*C*). Immunofluorescence also showed that the ratio

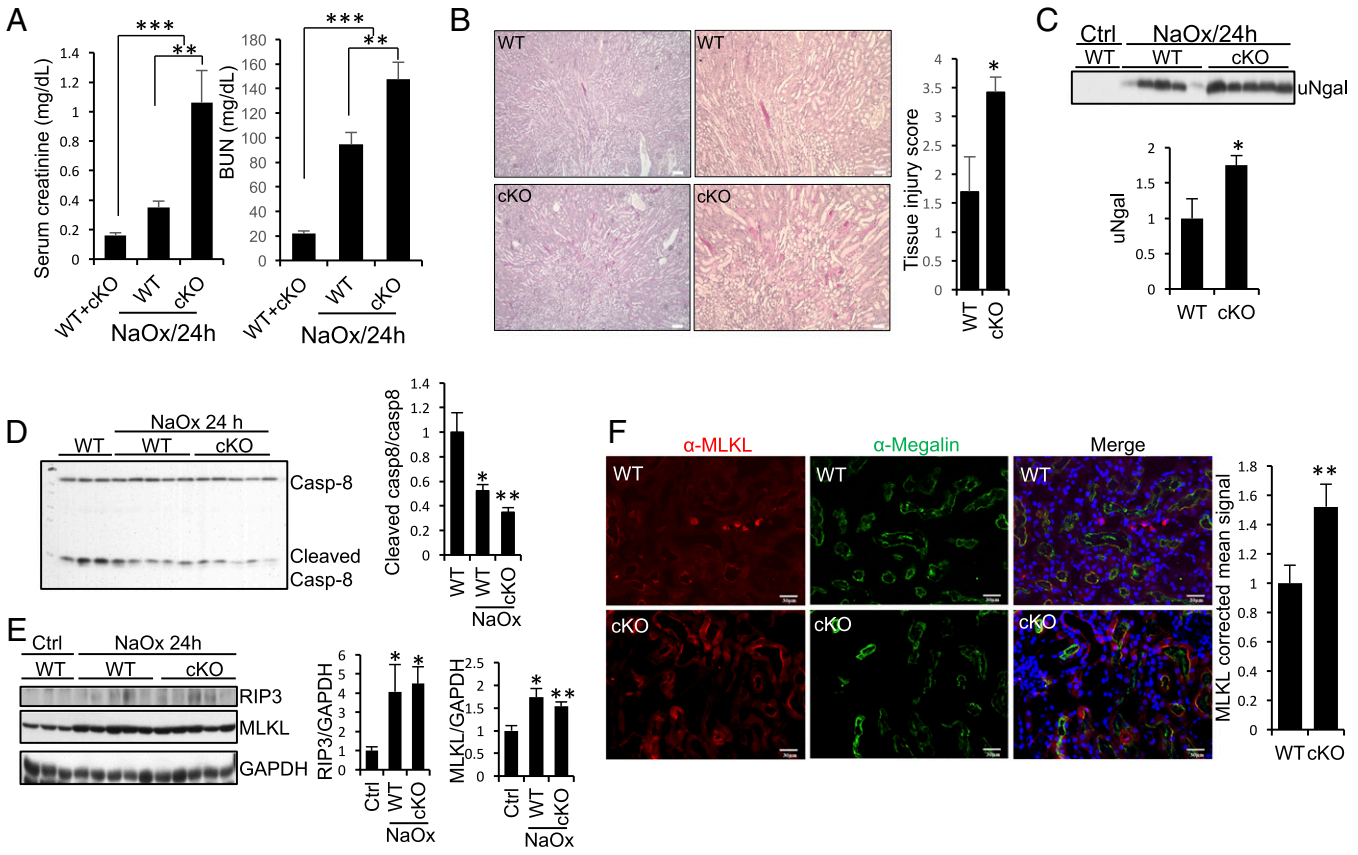

Fig. 4. Tubule-specific ablation of Rgmb aggravates crystal cytotoxicity. Male WT and Rgmb cKO mice at 2 mo of age were injected (i.p.) with NaOx at 100 mg/kg body weight. Mice were killed after 24 h. (*A*) Serum creatinine and BUN levels in WT and Rgmb cKO mice injected without and with NaOx. (*B*) PAS staining of kidney sections from WT and Rgmb cKO mice after NaOx injection. Representative photographs at different magnifications show more brush border loss, tubular dilation, tubular cell depletion, and cast formation in Rgmb cKO mice than in WT mice. Quantitative assessment of tubular injury is presented. (*C*) Excreted Ngal in urine in WT and Rgmb cKO after NaOx injection. Urine samples were subjected to Western blotting for Ngal (*Upper*) and quantified by densitometry (*Lower*). (*D*) Cleaved caspase-8 levels in kidneys after NaOx injection. Kidney lysates collected 24 h after NaOx injection were subjected to Western blotting using an antibody that recognizes both full-length and Casp-8. Cleaved caspase-8 levels relative to full-length caspase-8 levels were quantified by densitometry. (*E*) Expression of RIP3 and MLKL in the kidneys of WT and Rgmb cKO after NaOx injection. Kidney lysates from WT kidneys and injured kidneys were subjected to Western blotting for RIP3 and MLKL. RIP3 and MLKL levels relative to GAPDH levels were quantified by densitometry. (*F*) Cellular localization of MLKL in the outer medulla of WT and Rgmb cKO kidneys after NaOx injection. Immunofluorescence was performed for MLKL (red). Costaining with megalin (green) was included to identify proximal tubules. Outer medulla is presented. MLKL apical signal was quantified by ImageJ. GAPDH was used as the loading control for Western blotting. $n = 7$ for *A*; $n = 5$ for *B* and *F*. $^{*}P < 0.05$; $^{**}P < 0.01$; $^{***}P < 0.001$.

of cells with TSZ-induced phospho-MLKL plasma membrane localization was reduced by RGMb overexpression (Fig. 7*D*). Interestingly, membrane-associated MLKL was also reduced by RGMb-TM (Fig. 7*E*). These results suggest that RGMb does not affect MLKL phosphorylation and oligomerization, but inhibits its membrane translocation or membrane binding.

RGMb Does Not Regulate Ferroptosis. Ferroptosis has been reported to contribute to acute kidney injury (7, 58, 59). We examined the effects of inhibition of system x^-_c by erastin on cell death in HK-2 cells. Erastin dose-dependently induced cell death (*SI Appendix*, Fig. S18*A*), which was prevented by iron chelation with desferoxamine (DFO) or by Fer-1 (*SI Appendix*, Fig. S18*B*). Thus, HK-2 cells are sensitive to erastin-induced ferroptosis. Transfection of Rgmb into HK-2 cells did not alter erastin-induced ferroptosis (*SI Appendix*, Fig. S18*C*) although RGMb protein was expressed (*SI Appendix*, Fig. S18*D*). These results suggest that RGMb does not play a role in ferroptosis.

Discussion

Previous studies have demonstrated that TKPTS, HK-2, and NRK-52 tubular epithelial cells, or isolated proximal tubules, undergo necroptosis in response to various treatments (5, 6, 37, 38, 60). However, whether necroptosis occurs in renal tubules in vivo is questioned by a study showing that conditional deletion of FADD or caspase-8 in renal tubules did not induce spontaneous necroptosis under basal conditions (58). In the present study, we found that RIP3 and MLKL were induced during kidney injury induced by IR or oxalate cytotoxicity, while caspase 8 cleavage was inhibited. Importantly, MLKL was induced to be expressed on the apical membrane of proximal tubules, and inhibition of necroptosis by necrostatin-1 or GSK′963 dramatically reduced this expression and ameliorated tubular injury. MLKL permeabilizes and ruptures the plasma membrane once it binds to cell membrane (20, 21, 23–25). Therefore, our results demonstrate that necroptosis occurs in proximal tubular cells at least in the mouse models of IRI and oxalate nephropathy.

In normal kidneys, RIP3 and MLKL expression was not detectable. These results may explain the failure of FADD or caspase-8 deficiency to induce spontaneous necroptosis in renal tubular cells under basal conditions (58): Necroptosis could not take place when RIP3 and MLKL are not available although the necroptosis inhibitor FADD or caspase-6 is removed. Combing this previous observation with our own results, we hypothesize

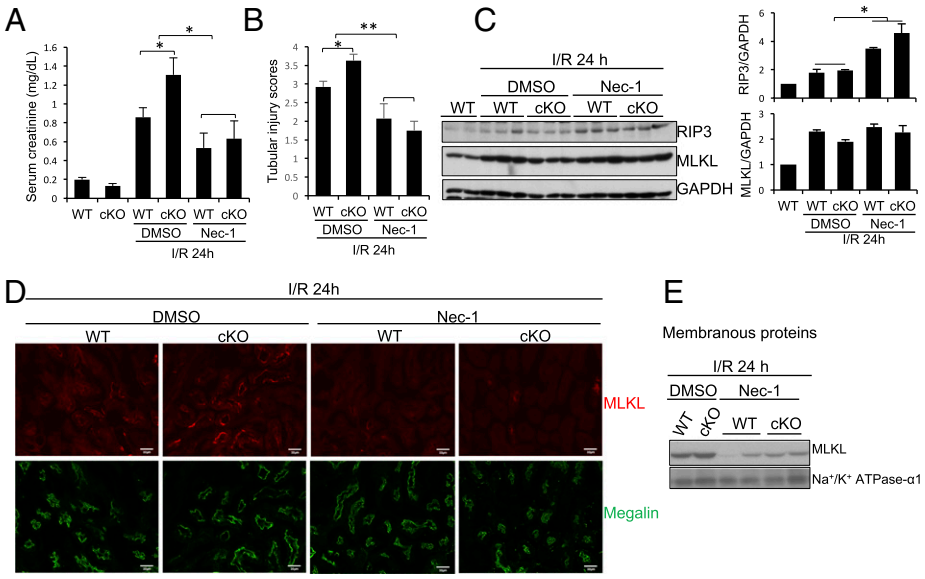

Fig. 5. Necrostatin-1 reduces MLKL expression on the apical membrane of proximal tubules and ameliorates IRI. Male WT and Rgmb cKO mice at 2 mo of age were injected with the vehicle (DMSO) or necrostatin (Nec)-1 (1.65 mg/kg body weight) 30 min before they underwent 40 min of bilateral renal pedicle clipping. Mice were killed 24 h after reperfusion. (*A*) Serum creatinine levels were measured in WT and Rgmb cKO mice. (*B*) Tubular injury scores were presented. (*C*) Expression of RIP3 and MLKL protein expression. Kidney lysates were used for Western blotting analysis for RIP3 and MLKL. RIP3 and MLKL levels relative to GAPDH levels were quantified by densitometry. (*D*) Immunofluorescence for MLKL and megalin in the outer medulla of kidneys from WT and Rgmb cKO mice injected with DMSO or Nec-1 before I/R. (*E*) MLKL levels in membranous fractions. Membranous proteins were isolated from kidneys of WT and Rgmb cKO mice with IRI, treated with and without Nec-1, and were subjected to Western blotting for MLKL. α1-subunit of Na^+/K^+ ATPase was used as the control for membranous proteins. $n = 6$–10 for *A* and *B*; $n = 5$ for *D*. $^*P < 0.05$; $^{**}P < 0.01$.

that the necroptotic pathway may not play a role in tubular cell homeostasis in kidneys under basal conditions.

We found that deletion of Rgmb in tubular cells increased the expression of MLKL on the apical membrane of proximal tubules during IRI or oxalate nephropathy. Deletion of Rgmb also exacerbated tubular injury and kidney dysfunction. Necrostatin-1 or GSK′963 treatment reduced MLKL apical expression and tubular injury in both WT and Rgmb cKO mice. In vitro, we demonstrated that RGMb inhibited necroptosis in mouse TKPTS and human HK-2 renal proximal tubular cells and in HT-29 colonic epithelial cells. Importantly, we found that RGMb reduced membrane-associated MLKL although it did not alter MLKL expression, phosphorylation, and oligomerization. These results provide evidence that RGMb inhibits necroptosis in proximal tubular cells by preventing MLKL membrane association. In addition, since inhibition of necroptosis by Nec-1 or GSK′963 reduced tubular injury and serum creatinine to similar levels in WT and Rgmb cKO, necroptosis in proximal tubules induced by Rgmb deletion may play a major role in the increased IRI observed in Rgmb cKO mice.

How RGMb reduces MLKL membrane association remains unsolved yet. RGMb has a signal sequence at the N terminus and a GPI anchor motif at the C terminus. RGMb is associated with cell membrane through the GPI anchor (40, 43), and the membrane-bound RGMb functions as a coreceptor for BMP signaling and a ligand for neogenin (39, 61). In this respect, we found that membrane-bound RGMb inhibits necroptosis no matter whether it is anchored to the plasma membrane through the GPI motif or transmembrane domains. However, our preliminary results showed that RGMb may not act through the BMP or neogenin pathway to regulate MLKL membrane association and necroptosis. In addition, we did not observe any interaction between RGMb and MLKL by immunoprecipitation under the necroptosis induction condition.

We previously showed that less apoptosis was observed in the collecting ducts of kidneys subjected to UUO in heterozygous global Rgmb KO mice (45) or in Ksp-cre–mediated Rgmb conditional KO mice compared with WT mice. In the IRI model, no cleaved caspase 3 was detected in kidneys after IRI, an observation consistent with a previous study (6). These results indicate that there is no or minimal tubular cell apoptosis at least during the early stage of IRI. Therefore, it is not surprising that we did not see any effects of Rgmb deletion on caspase-3 cleavage in IRI. Our results also suggest that RGMb differentially regulates apoptosis and necroptosis, and the overall effects of RGMb may be cell type and injury type dependent.

Ferroptosis also plays a role in AKI (7, 58, 59). Ferroptosis occurs when GPX4 is inhibited at the expression level, by small molecules such as RSL3 or by unavailability of glutathione. Inhibition of the glutamate/cysteine antiporter, system x^-_c, by erastin or by glutamate reduces intracellular glutathione levels, thus also inducing ferroptosis (53, 54). Interestingly, a previous study demonstrated that there was a sustained decrease in glutamate in kidney tissues after IR (62). Our present study found that the expression of Slc7a11, a subunit of system x^-_c, and Gpx4 was markedly increased by IR. The changes in glutamate, Slc7a11, and Gpx4 do not appear to favor ferroptosis, thus the molecular mechanisms underlying ferroptosis during IRI remain to be elucidated. Nevertheless, no differences in Slc7a11and Gpx4 expression in the kidney were found between WT and Rgmb cKO mice, and RGMb did not alter erastin-induced ferroptosis in vitro. Therefore, RGMb may not play a role in ferroptosis during AKI.

Taken together, our results demonstrated that RGMb reduced membrane-associated MLKL and inhibited necroptosis in vitro. Deletion of Rgmb in renal tubular cells increased MLKL expression on the apical membrane of proximal tubules, and aggravated tubular injury and renal functional impairment in IRI or oxalate nephropathy. Inhibition of necroptosis by necrostatin-1 or GSK′963 reduced MLKL apical expression in proximal tubules and improved IRI. RGMb inhibits tubular cell necroptosis during AKI.

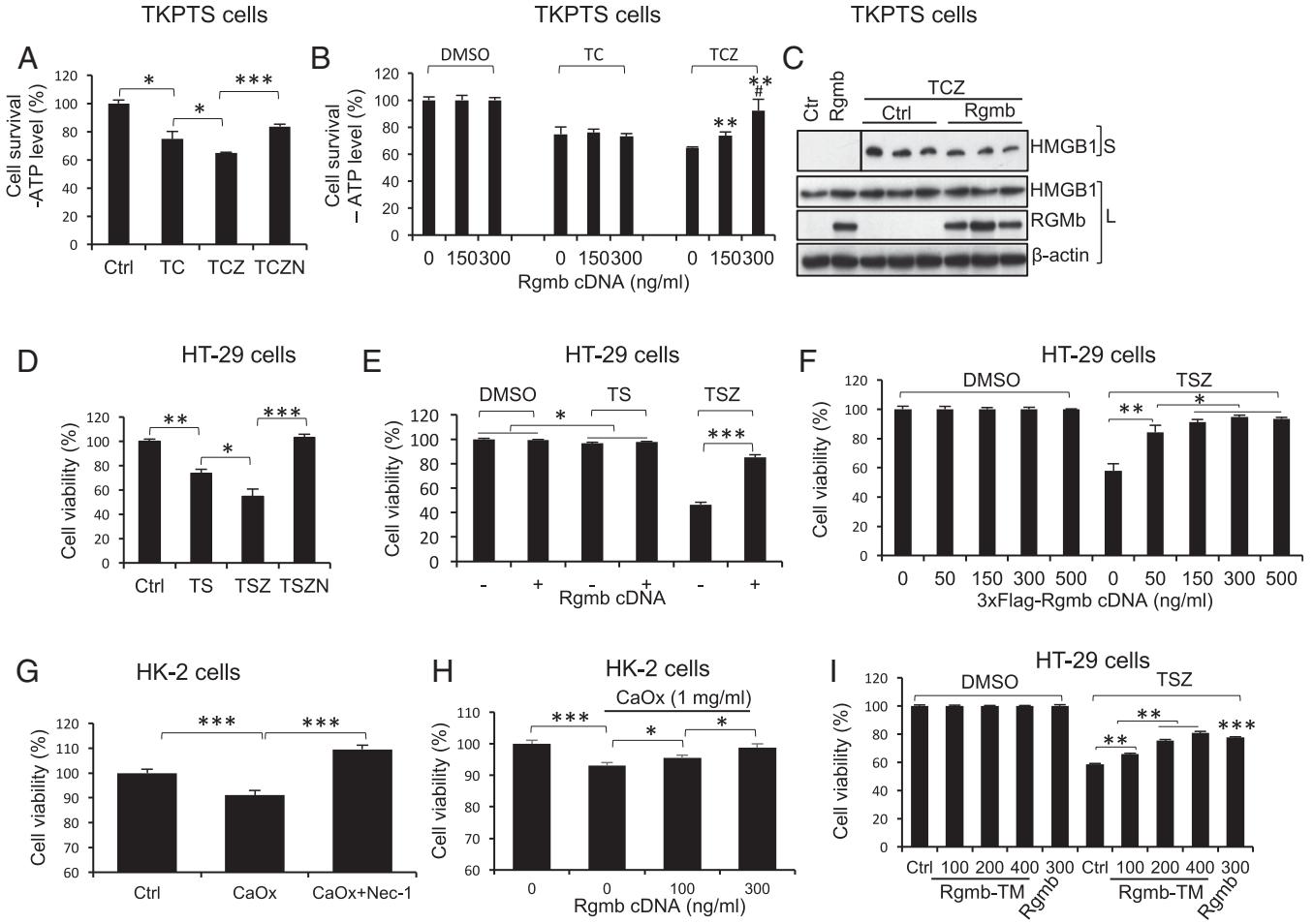

Fig. 6. RGMb inhibits necroptosis in TKPTS, HT-29, and HK-2 cells. (*A*) Necroptosis in TKPTS cells. Cells were treated with DMSO (Ctrl), TNF-α (100 ng/mL), CHX (2 μg/mL), zVAD-fmk (25 μM), and/or Nec-1 (50 μM) as indicated (TC, TCZ, or TCZN) for 24 h. Cell viability was measured using CellTiter-Glo Luminescent Cell Viability Assay. (*B*) RGMb inhibits TCZ-induced necroptosis but not TC-induced apoptosis in TKPTS cells. Cells were transfected with increasing amounts of Rgmb cDNA. Forty-eight hours after transfection, cells were treated with DMSO, TC (TNF-α and CHX), or TCZ (TNF-α, CHX, and zVAD-fmk) for 24 h before cell viability was measured. (*C*) RGMb reduces the release of HMGB1 from TKPTS cells in the presence of TCZ. Cells were transfected with or without Rgmb cDNA (300 ng/mL). Forty-eight hours after transfection, cells were treated with DMSO (lanes 1 and 2) or TCZ (lanes 3–8) for 24 h. Supernatants were collected and concentrated. Cells were lysed. Western blotting was performed for HMGB1 in supernatants and HMGB1 and RGMb in whole-cell lysates. β-actin was used as the loading control for cell lysates. (*D*) Necroptosis in HT-29 cells. Cells were treated with DMSO (Ctrl), TNF-α (30 ng/mL), the Smac mimetic Birinapant (50 nM), zVAD-fmk (20 μM), and/or Nec-1 (50 μM) as indicated (TS, TSZ, or TSZN) for 24 h. MTT assay was performed to determine cell viability. (*E*) RGMb inhibits TSZ-induced necroptosis but not TS-induced apoptosis in HT-29 cells. Cells were transfected with or without Rgmb cDNA (300 ng/mL). Forty-eight hours after transfection, cells were treated with DMSO, TS, or TSZ for 8 h before the cells were subjected to MTT assay. (*F*) RGMb dose-dependently inhibits necroptosis in HT-29 cells. Cells were transfected with increasing amounts of Flag-Rgmb plasmid. Forty-eight hours after transfection, cells were treated with DMSO or TSZ for 8 h before the cells were subjected to MTT assay. (*G*) CaOx crystals induce necroptosis in HK-2 cells. Cells were incubated with 1 mg/mL CaOx crystals in the absence or presence of Nec-1 for 24 h before cell viability was measured by MTT assay. (*H*) RGMb inhibits CaOx-induced necroptosis in HK-2 cells. Cells were transfected with increasing amounts of Rgmb plasmid. Twenty-four hours after transfection, cells were incubated with or without CaOx crystals for 24 h before cell viability was measured. (*I*) RGMb-TM inhibits TSZ-induced necroptosis. Cells were transfected with increasing amounts of Rgmb-TM cDNA (100, 200, and 400 ng/mL) or fixed amount of Rgmb cDNA (300 ng/mL). Forty-eight hours after transfection, cells were treated with DMSO or TSZ for 6 h before the cells were subjected to MTT assay. $n = 6$ for *A*, *B*, *D*, *F*, and *I*; $n = 3$ for *C*; $n = 10$ for *E* and *G*; $n = 8$ for *H*. $^{*}P < 0.05$; $^{**}P < 0.01$; $^{***}P < 0.001$. In *B*, ** indicates the differences between the doses 150 or 300 ng/mL with 0, and # indicates the difference between the doses 150 and 300 ng/mL.

Materials and Methods

See *SI Appendix, SI Materials and Methods* for detailed descriptions.

Generation of Renal Tubule-Specific Rgmb Knockout Mice. Floxed Rgmb mice on C57BL/6 background have been described (46). Excision of the loxP-flanked region in kidney tubular epithelial cells to establish conditional kidney knockout mice (cKO) was obtained by interbreeding with Ksp-Cre mice on the C57BL/6 background.

IRI. Bilateral IRI was performed as previously described with minor modifications (63). Briefly, male Rgmb cKO ($Rgmb^{f/f}$; Ksp-cre) mice and WT littermates ($Rgmb^{f/f}$, $Rgmb^{f/wt}$, or $Rgmb^{wt/wt}$; Ksp-cre) were placed on a heat plate at a temperature of 36.5–37 °C. Right and left flank incisions were made. The renal pedicles were clamped for 40 min, followed by reperfusion. The mice were killed at 24 h after ischemia. Mice with sham operation were used as control.

Necrostatin-1 was injected (i.p.) into mice 30 min before the mice were subjected to renal pedicle clamping. GSK′963 or its inactive enantiomer GSK′962 was injected (i.p.) 30 min before and 8 h after the ischemic surgery at the same dose of 2.5 mg/kg body weight.

All animal studies were approved by The Chinese University of Hong Kong Animal Experimentation Ethics Committee. Experiments were conducted in accordance with The Chinese University of Hong Kong animal care regulations.

Oxalate Nephropathy. Oxalate crystal kidney injury was performed as previously described (37). Male Rgmb cKO and WT littermates were injected

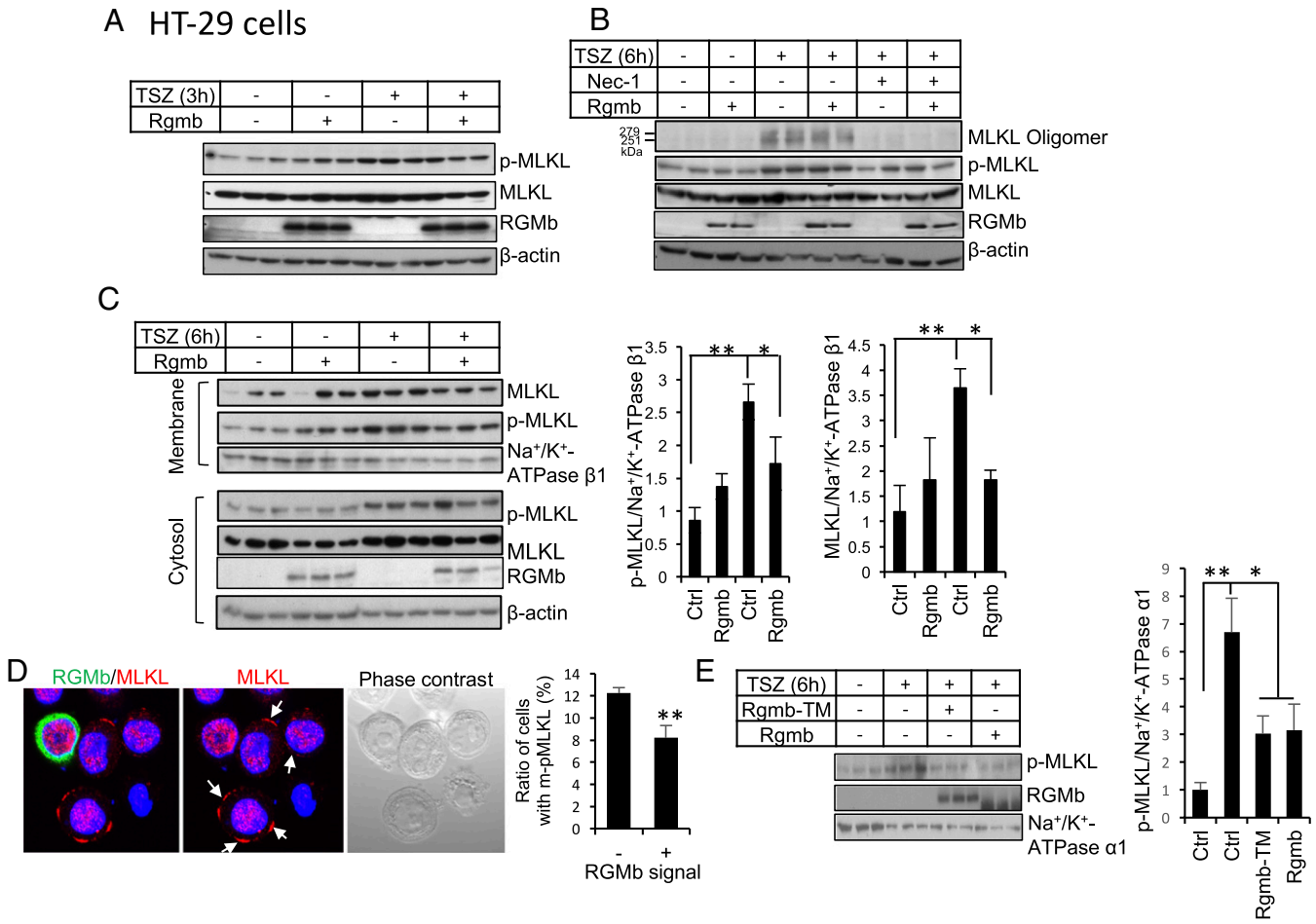

Fig. 7. RGMb reduces membrane-associated MLKL. (*A* and *B*) RGMb does not regulate MLKL phosphorylation and oligomerization. HT-29 cells were transfected with or without Rgmb cDNA (300 ng/mL). Forty-eight hours after transfection, cells were treated with or without TSZ (TNF-α at 30 ng/mL; the Smac mimetic Birinapant at 50 nM; zVAD-fmk at 20 μM) for 3 (*A*) or 6 h (*B*), in the absence or presence of Nec-1 (50 μM). Whole-cell lysates were subjected to Western blotting for MLKL, phospho-MLKL, and RGMb under reducing conditions, and for MLKL oligomers under nonreducing conditions. (*C*) RGMb reduces membrane-associated MLKL. HT-29 cells were transfected with or without Rgmb cDNA. Forty-eight hours after transfection, cells were treated with or without TSZ for 6 h. Membrane proteins and cytosolic proteins were isolated and subjected to Western blotting for MLKL, phospho-MLKL, and RGMb under reducing conditions (*Left*). Phospho-MLKL and MLKL relative to β1-subunit of Na^+/K^+ ATPase in the membrane fractions were quantified by densitometry (*Right*). β-actin was used as the loading control for cytosolic samples, and β1-subunit of Na^+/K^+ ATPase was used as the control for membrane proteins. (*D*) RGMb reduces the number of cells with phospho-MLKL plasma membrane localization. HT-29 cells were transfected with or without 3xFlag-Rgmb cDNA. Forty-eight hours after transfection, cells were treated with TSZ for 6 h. Immunofluorescence was performed for RGMb (green) and endogenous phospho-MLKL (red). Cells with plasma membrane MLKL were counted separately in 200–300 RGMb-negative cells and in 50–70 RGMb-positive cells. White arrows indicate phospho-MLKL expression in plasma membrane. The experiments were repeated three times. (*E*) RGMb-TM reduces membrane-associated MLKL. HT-29 cells were transfected with or without Rgmb-TM or Rgmb cDNA. Forty-eight hours after transfection, cells were treated with or without TSZ for 6 h. Membrane proteins were isolated and subjected to Western blotting for phospho-MLKL and RGMb (*Left*). Phospho-MLKL relative to α1-subunit of Na^+/K^+ ATPase in the membrane fractions were quantified by densitometry (*Right*). $^*P < 0.05$; $^{**}P < 0.01$.

(i.p.) with a single dose of sodium oxalate at 100 mg/kg body weight and provided with drinking water containing 3% sodium oxalate.

Histology and Immunofluorescence. Paraffin kidney sections were used for periodic acid-Schiff staining. The degree of tubular damage including tubular dilation, tubular atrophy, and cast formation was scored by three investigators without knowing the genotypes. Cryostat kidney sections were used for immunofluorescent staining to examine RGMb, megalin, RIP3, and MLKL cellular localization. MLKL fluorescence intensity on the apical membrane of PT cells was quantified by the ImageJ software.

Cell Culture and Transfection. Human colon carcinoma HT-29 cells were originally obtained from American Type Culture Collection. Mouse proximal tubular TKPTS cells were published previously (64) and were a generous gift from Rafia Al-Lamki, University of Cambridge, Cambridge, UK. TKPTS cells were maintained in DMEM/F12 (1:1) (Invitrogen) supplemented with 7% FBS and 1% SITZ liquid medium (Sigma-Aldrich). Human proximal tubular HK-2 cells were cultured in DMEM/F12 (1:1) medium supplemented with 10% FBS.

Cells were seeded in 6-, 12-, or 96-well plates and transfected with Rgmb or 3×Flag-Rgmb expression construct using Lipofectamine 2000 (Invitrogen). Transfected cells were incubated in completed medium for 1 or 2 d before experiments.

Necroptosis Induction. Necroptosis in TKPTS cells was induced by combined treatment with TNF-α, CHX, and the pan-caspase inhibitor zVAD. Necroptosis in HT-29 cells was induced by TNF-α, the smac mimetic Birinapant (S), and zVAD. Necroptosis in HK-2 cells were induced by CaOx crystals.

Isolation of Membrane Proteins. Cytosolic and crude membrane proteins from HT-29 cells and kidney tissues were performed as previously described (24). Briefly, HT-29 cells were washed with ice-cold PBS before the cells were harvested and permeabilized in a buffer containing 0.025% digitonin. The cortical and outer medullary region was dissected and homogenized in the same buffer. Cytosolic and crude membrane fractions were separated by centrifugation at 3,000 × *g* for 5 min. The supernatants were taken as cytosolic proteins. The pellets were washed with PBS and then solubilized to collect membrane proteins.

Statistical Analysis. All data are represented as mean ± SEM of independent replicates. Student's *t* test was applied for statistical analysis. A *P* value of less than or equal to 0.05 was considered statistically significant.

ACKNOWLEDGMENTS. We thank Dr. Jin-Fang Zhang (The Chinese University of Hong Kong) for providing HT-29 cells; Dr. Rafia S. Al-Lamki (University of Cambridge) for TKPTS cells; Dr. Susan Sou Ying Yung and Prof. Daniel Tak Mao CHAN (The University of Hong Kong) for HK-2 cells; Drs. John Bertin and Allison Beal (GlaxoSmithKline) for help with the experiments using GSK′963; Prof. Sudan He (Soochow University) for help with Western blotting on MLKL oligomers; and Prof. Junying Yuan (Harvard Medical School) for help with the detection of HMGB1 in cell culture. This study was supported by National Natural Science Foundation of China (NSFC)/Research Grants Council Joint Research Grants N_CUHK432/12 (to Y.X.) and 81261160507 (to B.Y.); CUHK direct Grant 4054305 (to Y.X.); NSFC Grant 81660120 (to W.L.); Science Foundation of Department of Education of Yunnan Province Grant 2016ZZX013 (to W.L.); General Basic Research Scheme of Yunnan Provincial Department of Science and Technology Grant 2017FB106 (to W.L.); National Cancer Institute Grant P50CA101942 (to G.F.); Deutsche Forschungsgemeinschaft Grants AN372/16-2, 20-1, 23-1, 24-1, and MU3906/1-1 (to H.-J.A. and S.R.M.); and General Research Fund (GRF) Grants 14121816 and C7018-16G (to H.-Y.L.).

1. Bonventre JV, Yang L (2011) Cellular pathophysiology of ischemic acute kidney injury. *J Clin Invest* 121:4210–4221.
2. Hotchkiss RS, Strasser A, McDunn JE, Swanson PE (2009) Cell death. *N Engl J Med* 361: 1570–1583.
3. Schumer M, et al. (1992) Morphologic, biochemical, and molecular evidence of apoptosis during the reperfusion phase after brief periods of renal ischemia. *Am J Pathol* 140:831–838.
4. Daemen MA, et al. (1999) Inhibition of apoptosis induced by ischemia-reperfusion prevents inflammation. *J Clin Invest* 104:541–549.
5. Linkermann A, et al. (2012) Rip1 (receptor-interacting protein kinase 1) mediates necroptosis and contributes to renal ischemia/reperfusion injury. *Kidney Int* 81: 751–761.
6. Linkermann A, et al. (2013) Two independent pathways of regulated necrosis mediate ischemia-reperfusion injury. *Proc Natl Acad Sci USA* 110:12024–12029.
7. Martin-Sanchez D, et al. (2016) Ferroptosis, but not necroptosis, is important in nephrotoxic folic acid-induced AKI. *J Am Soc Nephrol*.
8. Degterev A, et al. (2005) Chemical inhibitor of nonapoptotic cell death with therapeutic potential for ischemic brain injury. *Nat Chem Biol* 1:112–119.
9. Han J, Zhong CQ, Zhang DW (2011) Programmed necrosis: Backup to and competitor with apoptosis in the immune system. *Nat Immunol* 12:1143–1149.
10. Zhou W, Yuan J (2014) Necroptosis in health and diseases. *Semin Cell Dev Biol* 35: 14–23.
11. Linkermann A, Green DR (2014) Necroptosis. *N Engl J Med* 370:455–465.
12. Liu W, Xia Y (2016) Necroptosis in acute kidney injury. *Austin J Nephrol Hypertens* 3: 1059.
13. Galluzzi L, et al. (2012) Molecular definitions of cell death subroutines: Recommendations of the nomenclature committee on cell death 2012. *Cell Death Differ* 19: 107–120.
14. He S, et al. (2009) Receptor interacting protein kinase-3 determines cellular necrotic response to TNF-alpha. *Cell* 137:1100–1111.
15. Zhang DW, et al. (2009) RIP3, an energy metabolism regulator that switches TNF-induced cell death from apoptosis to necrosis. *Science* 325:332–336.
16. He S, Liang Y, Shao F, Wang X (2011) Toll-like receptors activate programmed necrosis in macrophages through a receptor-interacting kinase-3-mediated pathway. *Proc Natl Acad Sci USA* 108:20054–20059.
17. Sun L, et al. (2012) Mixed lineage kinase domain-like protein mediates necrosis signaling downstream of RIP3 kinase. *Cell* 148:213–227.
18. Zhao J, et al. (2012) Mixed lineage kinase domain-like is a key receptor interacting protein 3 downstream component of TNF-induced necrosis. *Proc Natl Acad Sci USA* 109:5322–5327.
19. Li J, et al. (2012) The RIP1/RIP3 necrosome forms a functional amyloid signaling complex required for programmed necrosis. *Cell* 150:339–350.
20. Cai Z, et al. (2014) Plasma membrane translocation of trimerized MLKL protein is required for TNF-induced necroptosis. *Nat Cell Biol* 16:55–65.
21. Chen X, et al. (2014) Translocation of mixed lineage kinase domain-like protein to plasma membrane leads to necrotic cell death. *Cell Res* 24:105–121.
22. Newton K, et al. (2014) Activity of protein kinase RIPK3 determines whether cells die by necroptosis or apoptosis. *Science* 343:1357–1360.
23. Wang H, et al. (2014) Mixed lineage kinase domain-like protein MLKL causes necrotic membrane disruption upon phosphorylation by RIP3. *Mol Cell* 54:133–146.
24. Hildebrand JM, et al. (2014) Activation of the pseudokinase MLKL unleashes the four-helix bundle domain to induce membrane localization and necroptotic cell death. *Proc Natl Acad Sci USA* 111:15072–15077.
25. Dondelinger Y, et al. (2014) MLKL compromises plasma membrane integrity by binding to phosphatidylinositol phosphates. *Cell Rep* 7:971–981.
26. Murphy JM, et al. (2013) The pseudokinase MLKL mediates necroptosis via a molecular switch mechanism. *Immunity* 39:443–453.
27. Rodriguez DA, et al. (2016) Characterization of RIPK3-mediated phosphorylation of the activation loop of MLKL during necroptosis. *Cell Death Differ* 23:76–88.
28. Ch'en IL, Tsau JS, Molkentin JD, Komatsu M, Hedrick SM (2011) Mechanisms of necroptosis in T cells. *J Exp Med* 208:633–641.
29. Trichonas G, et al. (2010) Receptor interacting protein kinases mediate retinal detachment-induced photoreceptor necrosis and compensate for inhibition of apoptosis. *Proc Natl Acad Sci USA* 107:21695–21700.
30. Dhib-Jalbut S, Kalvakolanu DV (2015) Microglia and necroptosis: The culprits of neuronal cell death in multiple sclerosis. *Cytokine* 76:583–584.
31. Dannappel M, et al. (2014) RIPK1 maintains epithelial homeostasis by inhibiting apoptosis and necroptosis. *Nature* 513:90–94.
32. Smith CC, et al. (2007) Necrostatin: A potentially novel cardioprotective agent? *Cardiovasc Drugs Ther* 21:227–233.
33. Kung G, Konstantinidis K, Kitsis RN (2011) Programmed necrosis, not apoptosis, in the heart. *Circ Res* 108:1017–1036.
34. Lin J, et al. (2013) A role of RIP3-mediated macrophage necrosis in atherosclerosis development. *Cell Rep* 3:200–210.
35. Welz PS, et al. (2011) FADD prevents RIP3-mediated epithelial cell necrosis and chronic intestinal inflammation. *Nature* 477:330–334.
36. Mocarski ES, Upton JW, Kaiser WJ (2011) Viral infection and the evolution of caspase 8-regulated apoptotic and necrotic death pathways. *Nat Rev Immunol* 12:79–88.
37. Mulay SR, et al. (2016) Cytotoxicity of crystals involves RIPK3-MLKL-mediated necroptosis. *Nat Commun* 7:10274.
38. Xu Y, et al. (2015) A role for tubular necroptosis in cisplatin-induced AKI. *J Am Soc Nephrol* 26:2647–2658.
39. Corradini E, Babitt JL, Lin HY (2009) The RGM/DRAGON family of BMP co-receptors. *Cytokine Growth Factor Rev* 20:389–398.
40. Samad TA, et al. (2004) DRAGON: A member of the repulsive guidance molecule-related family of neuronal- and muscle-expressed membrane proteins is regulated by DRG11 and has neuronal adhesive properties. *J Neurosci* 24:2027–2036.
41. Xia Y, et al. (2011) Dragon (repulsive guidance molecule b) inhibits IL-6 expression in macrophages. *J Immunol* 186:1369–1376.
42. Ma CH, et al. (2011) The BMP coreceptor RGMb promotes while the endogenous BMP antagonist noggin reduces neurite outgrowth and peripheral nerve regeneration by modulating BMP signaling. *J Neurosci* 31:18391–18400.
43. Xiao Y, et al. (2014) RGMb is a novel binding partner for PD-L2 and its engagement with PD-L2 promotes respiratory tolerance. *J Exp Med* 211:943–959.
44. Xia Y, et al. (2010) Dragon enhances BMP signaling and increases transepithelial resistance in kidney epithelial cells. *J Am Soc Nephrol* 21:666–677.
45. Liu W, et al. (2013) Dragon (repulsive guidance molecule RGMb) inhibits E-cadherin expression and induces apoptosis in renal tubular epithelial cells. *J Biol Chem* 288: 31528–31539.
46. Meng C, et al. (2016) Repulsive guidance molecule b (RGMb) is dispensable for normal gonadal function in mice. *Biol Reprod* 94:78.
47. Meng XM, et al. (2010) Smad2 protects against TGF-beta/Smad3-mediated renal fibrosis. *J Am Soc Nephrol* 21:1477–1487.
48. Zhou D, et al. (2012) Tubule-specific ablation of endogenous β-catenin aggravates acute kidney injury in mice. *Kidney Int* 82:537–547.
49. Patel V, et al. (2012) MicroRNAs regulate renal tubule maturation through modulation of Pkd1. *J Am Soc Nephrol* 23:1941–1948.
50. Shao X, Somlo S, Igarashi P (2002) Epithelial-specific Cre/lox recombination in the developing kidney and genitourinary tract. *J Am Soc Nephrol* 13:1837–1846.
51. Paragas N, et al. (2011) The Ngal reporter mouse detects the response of the kidney to injury in real time. *Nat Med* 17:216–222.
52. Bianchi ME, Manfredi A (2004) Chromatin and cell death. *Biochim Biophys Acta* 1677: 181–186.
53. Dixon SJ, et al. (2012) Ferroptosis: An iron-dependent form of nonapoptotic cell death. *Cell* 149:1060–1072.
54. Yang WS, et al. (2014) Regulation of ferroptotic cancer cell death by GPX4. *Cell* 156: 317–331.
55. Oberst A, et al. (2011) Catalytic activity of the caspase-8-FLIP(L) complex inhibits RIPK3-dependent necrosis. *Nature* 471:363–367.
56. Kaiser WJ, et al. (2011) RIP3 mediates the embryonic lethality of caspase-8-deficient mice. *Nature* 471:368–372.
57. Berger SB, et al. (2015) Characterization of GSK'963: A structurally distinct, potent and selective inhibitor of RIP1 kinase. *Cell Death Discov* 1:15009.
58. Linkermann A, et al. (2014) Synchronized renal tubular cell death involves ferroptosis. *Proc Natl Acad Sci USA* 111:16836–16841.
59. Friedmann Angeli JP, et al. (2014) Inactivation of the ferroptosis regulator Gpx4 triggers acute renal failure in mice. *Nat Cell Biol* 16:1180–1191.
60. Ouyang Z, et al. (2012) Necroptosis contributes to the cyclosporin A-induced cytotoxicity in NRK-52E cells. *Pharmazie* 67:725–732.
61. Bell CH, et al. (2013) Structure of the repulsive guidance molecule (RGM)-neogenin signaling hub. *Science* 341:77–80.
62. Wei Q, Xiao X, Fogle P, Dong Z (2014) Changes in metabolic profiles during acute kidney injury and recovery following ischemia/reperfusion. *PLoS One* 9:e106647.
63. Wei Q, Dong Z (2012) Mouse model of ischemic acute kidney injury: Technical notes and tricks. *Am J Physiol Renal Physiol* 303:F1487–F1494.
64. Arany I, Megyesi JK, Kaneto H, Tanaka S, Safirstein RL (2004) Activation of ERK or inhibition of JNK ameliorates H(2)O(2) cytotoxicity in mouse renal proximal tubule cells. *Kidney Int* 65:1231–1239.